Quaternary Geochronology 29 (2015) 36–47

Contents lists available at ScienceDirect

Quaternary Geochronology

journal homepage: www.elsevier.com/locate/quageo

Research paper

When were the walls of the Chauvet-Pont d'Arc Cave heated? A chronological approach by thermoluminescence

Pierre Guibert [a, *], Aurélie Brodard [a], Anita Quiles [b], Jean-Michel Geneste [c, d], Dominique Baffier [e], Evelyne Debard [f], Catherine Ferrier [c]

[a] IRAMAT-CRP2A (Institut de recherche sur les Archéomatériaux, Centre de Recherche en Physique Appliquée à l'Archéologie), UMR 5060 CNRS – Université Bordeaux Montaigne, Maison de l'Archéologie, F-33607 Pessac Cedex, France
[b] Pôle d'archéométrie – Institut Français d'Archéologie Orientale, 37 rue al-Cheikh Aly Youssef B.P. Qasr el-Ayni 1152, 11441 Le Caire, Egypt
[c] PACEA (de la Préhistoire à l'Actuel: Cultures, Environnement, Anthropologie), UMR 5199 CNRS – Université de Bordeaux, Avenue des Facultés, F-33405 Talence Cedex, France
[d] Centre National de Préhistoire, Ministère de la Culture et de la Communication, F-24 000 Périgueux, France
[e] Ministère de la Culture et de la Communication, Direction Régionale des Affaires Culturelles de Rhône-Alpes, CREPS, route de Salavas, F-07150 Vallon-Pont-d'Arc, France
[f] Laboratoire de géologie de Lyon: Terre, planètes et environnement (LGL-TPE), UMR 5276 CNRS – Université Lyon 1, F-69622 Villeurbanne Cedex, France

ARTICLE INFO

Article history:
Received 25 December 2014
Received in revised form
10 April 2015
Accepted 20 April 2015
Available online 28 May 2015

Keywords:
Chauvet-Pont d'Arc Cave
Thermoluminescence dating
Heated bedrock
Calcite
Disequilibrium in U series
Radon

ABSTRACT

Direct chronological data of the ancient heating of calcitic walls at the Chauvet-Pont d'Arc Cave (Ardèche, France) were obtained at the *Galerie des Mégacéros* and at the *Eboulis d'Entrée*. Fragments of reddened limestone were extracted from the walls and were studied by thermoluminescence (TL). A novel measurement protocol of the equivalent dose (ED) was implemented and was optimized with respect to the nature of the material being dated (calcite), to the small quantities of sample available and to the relatively low heating of the rock surface in the past (close to 350 °C). The presence of a high level of free radon in the cave and ^{210}Pb in large excess in samples implied the development of a specific irradiation model allowing the evaluation of the mean annual dose over time, taking into account possible scenarios of radon and daughters migration from the bedrock. The following dating results were obtained (in ka before the present and associated total estimated standard deviation):

- *Galerie des Mégacéros*, 36.9 ± 2.3 ka.
- *Eboulis d'Entrée*, 34.3 ± 2.9 ka.

These data are in agreement with the calibrated radiocarbon dates of the most ancient periods of human occupation in their respective areas. TL dates indicate that the fires which altered the walls were lighted during the first paleolithic human occupation period. Eventually, TL dating of the heated surface of the bedrock opens a new window on the chronology of human activities in the Chauvet-Pont d'Arc Cave and it makes an alternative contribution to the demonstration of the early chronology of its rock art.

1. Introduction

Since their discovery, the origin and the chronology of rock art representations of the Chauvet-Pont d'Arc Cave have been questioned. Indeed the initial chronology based on stylistic considerations disagreed with the first direct AMS radiocarbon dating of charcoal pigments (Valladas et al., 2001a). Recent debates continue to address the question of chronology (see the review paper by Pettitt, 2008) and inferences about the cognitive capacities of early upper Palaeolithic people. This controversial discussion with the Chauvet-Pont d'Arc team induced methodological questions about the consistency of stylistic attributions, about the appropriateness of linking the Chauvet-Pont d'Arc representations with other reference sites, whose chronology was supposedly better known. That is why, the Chauvet-Pont d'Arc scientific team is currently developing a methodological and integrated approach to dating, which includes different analysis methods, to restitute the cave not only in view of the human occupations but also in its environment.

* Corresponding author.
E-mail address: pierre.guibert@u-bordeaux-montaigne.fr (P. Guibert).

http://dx.doi.org/10.1016/j.quageo.2015.04.007
1871-1014/

Radiocarbon dating has been widely performed on charcoal species (direct dating of pigments, as well as charcoal pieces from hearths), bones (with a view to dating the animal occupation of the cave, and in particular those of cave bears) and rock paintings. Radiocarbon results were compared between international independent laboratories (Cuzange et al., 2007; Quiles et al., 2014) to test the accuracy of the method, and were corroborated by other dating techniques, for instance U–Th dates on speleothems (Valladas et al., 2001a, b; 2005; Genty et al., 2004; Bocherens et al., 2005; Cuzange et al., 2007; Quiles et al., 2014). A recent study has used cosmogenic isotopes formed in the limestone to date the last events in the collapse of the cliff. It has shown that the closure of the Cave which has been associated with the last rockfall, occurred around 21.5 (±1.0) ka (Sadier et al., 2012). This last result is coherent with the fact that there are no more recent remains of large mammals. This chronology excludes definitely the assumption of Magdalenian representations that was first evoked upon the discovery of the Cave (see the review paper by Pettitt, 2008). The whole dating results gives a thorough and precise idea of the chronology of both human and animal occupations. In spite of that, the chronological attribution of the most ancient representations to the first Prehistoric occupation still remains uncertain.

This present study aims to provide new information about the chronological frame of the Palaeolithic occupation of the Chauvet–Pont d'Arc Cave by using thermoluminescence method applied to reddened fragments of limestone. The demonstration of wall burning (Ferrier et al., 2014; Brodard et al., 2014) gives new insights into the cave occupation and the processing of walls by the Palaeolithic people. Heating marks, such as rubefaction and desquamation, are the results of a thermal treatment of anthropic origin. These marks of heating are open to direct TL dating. We propose to build a new chronological window into the Chauvet-Pont d'Arc Cave history, independent from the other dating methods applied there.

2. Samples

Besides conservative considerations, the sampling constraints were essentially founded on the absence of visible secondary crystallization (posterior to the supposedly thermal treatment) on the calcite fragments. Another main point was to avoid any invasive extraction of material from the walls, and particularly in the vicinity of drawings or engravings, where the removal would have been too visible. After receiving due permission from the Chauvet-Pont d'Arc Cave Curator, small fragments of limestone were then sampled at the *Galerie des Mégacéros*, at the *Diverticule des Ours* and at the Paleolithic Entrance of the cave. They all present a light reddened coloration, in comparison with the natural Urgonian limestone, which is rather light beige. Most of those limestone fragments were collected on the archaeological soil, but two were sampled from their original place on the wall of the *Galerie des Mégacéros* (BDX 14338) and from the ceiling of the *Eboulis d'Entrée* (BDX 14341). In addition a larger piece of unheated limestone was collected on the floor of the entrance scree in order to build thermal references from the same geological material as the archaeological ones under study. Table 1 summarizes the characteristics of samples and Fig. 1 shows their location in the karstic network of the Chauvet-Pont d'Arc Cave, as well as the areas where heating marks were observed.

The main result of the thermal study by thermoluminescence (Brodard et al., 2014; Ferrier et al., 2014) was that most of the samples were heated in the past at around 300–375 °C (equivalent to 1 h at 300–375 °C in air). In order to complete the demonstration of a heating process by the Palaeolithic people, a full thermoluminescence study of the two fragments BDX 14338 and BDX 14341 was carried out, but beyond this thermal characterization study, chronological information on anthropic alterations of the walls are provided.

About the relations with the representations, in the *Galerie des Mégacéros* there is no direct stratigraphical link between the sample collected on the wall with the parietal art in the vicinity, nor in the Entrance, where there is no trace of painting or engraving. But, in the *Galerie des Mégacéros*, two representations attributed as being Aurignacian in origin (rhinoceros and a pubic triangle) are superimposed with a reddened coloration of the wall. At other places, there are some clear links with the representations, for example the bears at the *Diverticule des ours*, were painted on an already heated and reddened wall. Intentional choice or not for a colored support, in this case, the relative chronology between fires and painting is clear. In addition, both examination of the type of Bear represented and DNA analyses of the bear remains found in the Chauvet-Pont d'Arc Cave suggest that only Aurignacian artists would have been able to draw those representations (Bon et al., 2011; Ferrier et al., 2014). These observations suggest that some of the thermal alterations could have taken place within the oldest period of human occupation of the cave. But finally at this point of investigation, we must consider that the fires at the origin of these thermal alterations were independently lighted and should not be considered as contemporary.

The Urgonian limestone which is the mineral support of the Chauvet rock art is principally composed of calcite. It is a compact rock of low porosity, and the detritic phases, including quartz, are at a trace level (0.4–0.6% of unsoluble matter in HCl). Consequently, calcite was the basic mineral of our TL study. It should be stressed that the use of calcite as a natural dosimeter in luminescence dating is not as common as quartz (or more generally silicated minerals, like feldspars), and we found it useful to recall at this point some luminescence properties of dating interest.

3. Thermoluminescence dating of calcite

First of all, the luminescence spectrum of calcite from limestones, speleothems and marbles, is mainly dominated by the orange emission of Mn^{2+} around 600 nm (Townsend et al., 1994; Macedo et al., 1999; Silletti et al., 2012). A near UV/violet component has also been reported in literature, and unlike the orange emission, its physical origin is not yet clearly identified.

In practice, the glow curve of calcite is composed of 3 main parts as reported by many authors (Carmichael et al., 1994; Franklin et al., 1990; Townsend et al., 1994; Pagonis and Michael, 1994; Engin and Güven, 1997, 2000; Ninagawa et al., 2001; Roque et al., 2001a, b; Ponnusamy et al., 2012). The temperature ranges listed below depend on the heating rate that varies between 1 and 10 °C/s according to authors and studies: i) a low temperature component, between ca. 100° and 200 °C with a maximum culminating around 150 °C. These low temperature signals are only visible with laboratory irradiation because of their short lifetimes. ii) A medium temperature region, between 250° and 300 °C where a marked TL peak around 280 °C is generally observed. This component can be made of several contributions, according to the samples, nature and content of contributing centers to the TL. iii) A high temperature emission, above 320 °C, with a peak around 360 °C.

The glow curve shape of calcite is found rather uniform in comparison with that of quartz which can exhibit significant differences according to radiation and thermal history of samples. This is also due to the nature of impurities that play a role in the luminescence properties. The medium and high temperature regions are of dating interest. Mainly, the ca. 280 °C TL peak of calcite is generally used for dating. Once the calcite is completely zeroed, the growth of the 280 °C peak is generally found to be

supralinear, but on the opposite the high temperature component, TL emission around 350 °C, exhibits an early saturating growth with the dose. The uncommon growth of these two components of the calcite TL is governed by at least two different traps in competition, and their behavior is satisfactorily described by the so-called competing trap model (Ninagawa et al., 1994, 2001). Anyway, it is a common experience to notice that the high temperature emission is often more problematic to exploit than the 280 °C peak. This is mainly due to the superimposition of spurious luminescence signals generated by heating. Amongst various interpretations, the following are meaningful for our purposes: i) decarbonation of the surface of already heated calcite grains (Roque et al., 2001a), that is stopped by using a CO_2 atmosphere while heating calcium carbonate samples. ii) Pyrolysis (thermal cracking of organic matter trapped in calcite crystals, like transitions from alkyl molecular radicals to perynaphthenyl ones observed by Electron Spin Resonance (ESR) in flints; Duttine et al., 2005, Joannes-Boyau et al., 2014), that can generate weak luminescence emissions. iii) Dehydroxylation of traces of hydrocalcite or thermal desorbtion of water molecules from the surface of calcite grains, deduced from losses of mass around 360 °C observed in coupled Thermo Gravimetric Analysis – Gas Analysis accompanying the thermal transition aragonite-calcite in corals (Ganteaume et al., 1990), or more simply the heating of calcite itself (Ponnusamy et al., 2012).

In addition, some authors observed “recuperation” signals instead of pure background, after measuring the natural TL of previously unheated materials such as shells (from irradiated shell fish, Carmichael et al., 1994), speleothem calcite (Engin and Güven, 2000), natural calcite crystals from India (Ponnusamy et al., 2012). The nature of these spurious phenomena is not clearly understood yet, even if some of these observations can be attributed to the cracking of organic matter and the production of unstable radicals that interact with the mineral lattice in the case of unheated natural materials submitted to TL experiments. This process must be differentiated from the “recuperation TL” of marble calcite after optical bleaching (Polikreti et al., 2003) that is surely identified as a thermal transfer of charges from optical traps to shallower ones displaced by the exposure to light, and then reworked by preheating or mid-term storage at room temperature (RT).

The long-term stability of the 280 °C TL peak and its ability to dating was questioned by some authors, because of the relatively low temperature of emission. In the present case, this is also one of our questions, since the expected ages are in the 20–40 ky range. Many works were undertaken by different groups and they all demonstrate that the activation energy of this peak is sufficiently high to be suitable for dating purposes: around 1.7 eV (Pagonis and Michael, 1994; Engin and Güvin, 1997) giving RT extrapolated lifetimes around 15–20 Ma. Indirect demonstration of the dating capacity was supported by the comparison between results from TL-dating of calcite and other dating techniques or materials: for instance, Ninagawa et al. (2001) get a satisfactory agreement between TL of calcite and U–Th measurements when the 280 °C peak has a supra-linear growth for ages as old as 200 ka, Roque et al. (2001a), obtained a good agreement between C14 and TL-dating of heated limestones at Combe-Saunière (Dordogne, France) for Upper Paleolithic levels, and also at Laugerie-Haute (Dordogne, France) for Solutrean layers (20–22 ka) in comparison with C14 ages on burnt bones or TL ages of heated quartz pebbles (Roque et al., 2001b).

Concerning the sensitivity changes of calcite with thermal annealing, a topic of interest in the study of the thermal characterization of the Chauvet samples, the behavior reported is common in all the studies made on initially unheated materials. The TL sensitivity of the orange emission gradually increases and a maximum is attained around 600 °C (1 h in air in Engin and Güven, 2000) then drops at higher annealing temperatures (700–750 °C observed by Franklin et al., 1990; Pagonis et al., 1994: Engin and Güven, 2000; Ponnusamy et al., 2012). In addition, Engin and Güven (2000) first, then Ponnusamy et al. (2012) observed a relationship between cooling rate and sensitivity: the more rapid the cooling rate, the greater the TL sensitivity. An attempt at physical interpretation was given by these authors, referring to research by Nakajima (1971) who stated that the OH group acts as a luminescence killer. As the annealing temperature increases, OH groups recombine and give H_2O molecules that leave the calcite crystals (inducing sensitivity increase), but beyond 600 °C the decarbonation process debutes and after cooling, new OH groups are formed by interaction between high temperature heated calcite and the humidity of the air (explanation of the subsequent drop in sensitivity). On the basis of annealings made in air or CO_2 or N_2, Pagonis (1998), proposed that the reduction of sensitivity beyond 650 °C should be the result of the oxidation of the luminescence center Mn^{2+} in air.

Table 1
List and characteristics of collected samples for thermal history characterization and dating. Equivalent paleotemperatures were determined by TL (details in Ferrier et al., 2014).

Sample references	Location	Comments	Range of equivalent heating temperature
Galerie des Mégacéros			
TL#1-2010/BDX 14338	Reddened wall	Reddened chip (ca. 4 mm thick, 30 × 60 mm^2) at 1.8 m high from archaeological soil	325–375 °C
TL#2-2010/BDX 14339	Soil	Chip collected on the soil, at the base of the reddish zone where was taken BDX 14338 (ca. 4 mm thick, 20 × 20 mm^2)	325–375 °C
TL#3-2012/BDX 15891	Soil	Grey chip collected on the soil (ca. 4 mm thick, 20 × 30 mm^2), near a fallen limestone block, under the metallic footpath	ca. 450 °C
Diverticule des Ours			
TL#3-2010/BDX 14340	Soil	Small red limestone flake on soil near the location of a charcoal sample C14 GC 0803 (ca. 3 mm thick, 15 × 15 mm^2)	300–350 °C
TL#1-2012/BDX 15889	Sol	Small red limestone flake on soil, entrance of the chamber (ca 3 mm thick, 30 × 20 mm^2)	300–350 °C
TL#2-2012/BDX 15890	Wall	Small fragment from a red zone on the right wall of the chamber entrance (ca. 4 mm thick, 4 × 8 mm^2)	Sample showing saturated TL signals but heated-like shape of glow curve (ca. 300 °C)
Eboulis d'Entrée, Entrance scree			
TL#4-2010/BDX 14341	Ceiling	Small reddened fragment from the ceiling of the paleolithic entrance, ca. 1.5 m from the current soil (ca. 5 mm thick, 30 × 40 mm^2)	325–375 °C
TL#5-2010/BDX 14342	Soil	Unheated limestone fragment used as reference material in this work (15 mm thick, 10 × 15 cm^2)	Not heated

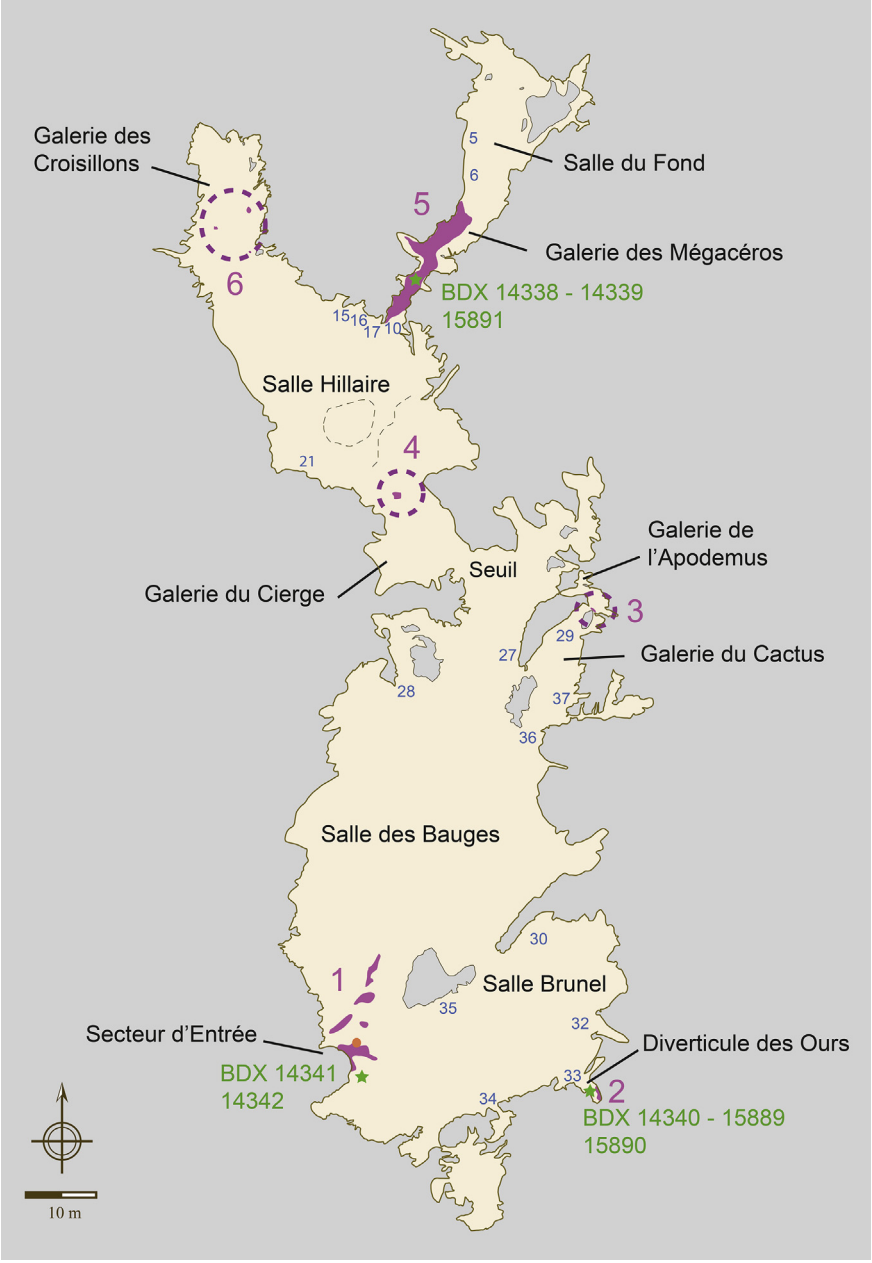

Fig. 1. Map of Chauvet-Pont d'Arc Cave and sample location (from Y. Le Guillou and F. Maksud). Reddened zones in purple; green stars: location of TL samples with their laboratory references.

4. Instruments, sample preparation and protocols

4.1. Determination of equivalent doses: instruments and protocols

TL measurements of the Chauvet samples were recorded with an automated TL-reader built in IRAMAT-CRP2A (Guibert, 2002). The following conditions (see Roque et al., 2001a) were applied: all heatings were undertaken at a rate of 4 °C/s in wet CO_2 atmosphere (CO_2, 4% H_2O vapor); the spectral window was selected from 470 to 550 nm (A520 MTO green filter and an IR rejector optical filters; phototube EMI 9813 QKA). It allows the recording of the emitted TL by high energy photons of the Mn^{2+} emission spectral peak. Laboratory irradiations were given by a ^{90}Sr–^{90}Y beta source delivering ca 0.075 Gy/s (±2.5%) and an external ^{241}Am alpha source delivering 0.17 Gy/s (±5%).

TL dating concerns two fragments of reddened calcite that were taken from their original position on the wall of the *Galerie des Mégacéros* (BDX 14338) and from the ceiling of the paleolithic entrance (BDX 14341). We distinguished two separate sub-samples for those 3–4 mm thick fragments: the side in contact with the bedrock, and the "external side", facing the gallery. Subsamples will be named by adding the index "b" or "e" to their identification number. Each side was grated to around 1 mm thick and the limestone powder was produced. The less than 40 μm fraction was kept and washed according to the following cleaning protocol: the grains are washed by demineralized water and then submitted to the oxidizing action of a concentrated solution of H_2O_2 for 2 days (elimination of organic molecules from the surface of the grains). The 3–12 μm fraction was selected by sedimentation in acetone and deposited onto brass platelets (equivalent thickness 0.5–1 mg/cm^2).

The protocol used to date the calcite fragments takes account of both the small quantity of material, and the relatively low equivalent temperature of heating (equivalent to 1 h in air at between 300 and 375 °C, Brodard et al., 2014). We then imagine a protocol derived from the SAR technique, the characteristic point of which is the direct comparison between natural signals and regenerated ones. It has been called MANARS, as Multi Aliquot Natural Annealing Regeneration Sensitivity. The heating at low temperature was taken as an advantage since we have been able to reproduce, by the inherent heating of TL experiments, a close approach of the archaeological resetting of traps. Indeed, we know that SAR TL is often problematic with high fired materials such as quartz (Bassinet et al., 2006; Guibert et al., 2009a), and many studies by our group have shown that the thermal resetting is an important point to consider. So thermal zeroing in the usual TL MAAD (Multi Aliquot Additive Dose) protocols with a view to reconstructing the growth curve of TL with the dose should be defined with particular attention. In practice, different annealing conditions of grains are chosen and the one that gives the least sensitivity variations and changes in the shape of the glow curve is selected (more details for different situations in Roque et al., 2004; Duttine et al., 2005; Blain et al., 2007), and the rest of the experiments, including the second reading of TL after annealing, are undertaken. Here, with a SAR-like protocol we checked the adequacy of heating in the TL apparatus as a convenient annealing of grains and the meaningful parameter was the maximal temperature attained by keeping the heating rate constant. The general protocol used for ED and the alpha radiation relative efficiency measurements is given in Table 2 and in supplementary tables S1 and S2. We recall that, in general, for a given a constant dose, the alpha irradiation induces a lower TL intensity than beta or gamma ones. The ratio is around 10% and even generally lower for quartz OSL, around 3–5%, meaning that alpha particles are much less efficient to produce TL than beta particles or gamma rays (see for instance Aitken, 1985 for a comprehensive explanation and Brennan et al., 1991 for the dependence with the grain-size).

Unlike quartz OSL, the TL of heated calcite is generally homogeneous within grains. Moreover, as thousands of fine grains are deposited on platelets, the dispersion of TL intensities between different aliquots is very low. That's why we normalized all signals by the natural TL signal. At last, we build the growth curve by plotting laboratory dose as a function of the ratios of TL, $X_i = R_i/N_i$, (R_i is the regenerated signal of the ith aliquot, N_i its natural TL signal) the variation of which is fitted by polynomials. The growth of TL with the dose being in general supra-linear due to the competing traps charge filling mechanism already mentioned, the usual saturating exponential function widely used for quartz OSL is not available with calcite TL. The ED is given by summing the coefficients of corresponding polynomials (taking X = 1).

The procedure used allowed us to check for the existence of sensitivity changes and of predose effects: one of the regenerative doses is taken as equal to the test dose D_0 (58Gy) given at the end of the cycle for each aliquot (Table 2). Due to the role of this elevated test dose, changes in sensitivity can then be easily controled, by comparing the signals induced by the lower regenerative dose and that of the test dose D_0. Predose effects were monitored as well, by plotting the ratio T_i/N_i as a function of the regenerative dose administrated before applying the test-dose D_0, T_i being the TL signal of the ith aliquot generated by the test dose. In addition, we performed also dose recovery tests by adding a beta dose, D_{Rec}, to a series of naturally irradiated aliquots. We used the same protocol as in Table 2 for ED measurements, except that a beta dose D_{Rec} close to the archaeological dose was given to the aliquots before recording their first glow curve ($N + D_{Rec}$). The alpha efficiency (k-factor) was evaluated in two different ways (see supplementary tables S1 and S2): the first one (mode 1) by adding a constant alpha dose to naturally irradiated aliquots, the second one (mode 2) by giving an alpha irradiation of aliquots that were already thermally reset after recording their natural TL and corresponding background.

4.2. Determination of annual dose rates

The dose rates of the calcite fragments were determined from radioanalytical measurements (Guibert et al., 2009b) using conversion factors by Guérin et al. (2011) and taking account of the alpha efficiency (k-factor in the present work) measured for any sample, and from gammametric measurements made in the cave at the precise sampling locations. Additional characterization of radioactivity was carried out by beta autoradiography. K, U, Th and disequilibria in U-series were measured by high resolution γ spectrometry. We used a U-shape well Ge detector (Eurisys Mesures, EGPC 200 P17), the active volume of which is 200 cm^3 and the well dimensions are 17 mm in diameter and 50 mm in depth. The detector is shielded by 15 cm of low and ultra-low activity lead and ultrapure copper rings. The signal is processed by an 8 k

Table 2
Sequential protocol for ED determination and added dose recovery tests. The additive dose given to aliquots for the Dose Recovery experiments, D_{Rec}, is taken close to the natural dose of samples or subsamples considered. The regenerative dose series at step 5 vary according to the samples so that the variation interval of regenerated doses includes the natural dose or the [Nat + D_{Rec}] one.

ED measurement and additive dose recovery tests protocols
For aliquot i, from i = 1 to N
1 This step only in case of Dose Recovery Test: irradiating at RT by a dose DRec; with DRec = {117Gy (BDX 14338b and e), 175Gy (BDX 14341e), 87.5Gy (BDX 14341b)}
2 Preheating 210 °C (cutheat);
3 Heating from RT to 420 °C: measurements of Nat TL signals or [Nat TL + D_{Rec}] signals if DRT protocol;
4 Heating from RT to 420 °C: "background" measurement;
5 Beta irradation a with regenerative dose Di:
- In case of ED measurement: D_i = {58, 117, 175, 58, 87, 117, 175, 233* Gy} (* for BDX 14341 only);
- In case of additive DRT experiment: D_i = {175, 233, 233, 292 Gy} for BDX 14338b and e; {292, 350, 350, 408 Gy} for BDX 14341e; {146, 175, 175, 204 Gy} for BDX 14341b;
6 Preheating 210 °C (cutheat);
7 Heating from RT to 420 °C: regenerated TL measurements;
8 Heating from RT to 420 °C: "background" measurement;
9 Beta irradation with a test dose D_0 (58 Gy);
10 Preheating 210 °C (cutheat);
11 Heating from RT to 420 °C: test dose TL measurements;
12 Heating from RT to 420 °C: "background" measurement;
Next aliquot;

channel analyzer.

The inner part and the rest of the samples to be dated were crushed and homogenized. A part of the unheated reference material was powdered in totality including external faces. With a view to gamma spectrometric measurements in the well detector, the powder obtained was introduced into polythene tubes (16 mm external diameter, 12 mm internal diameter, 55 mm high) and sealed. After the physical preparation process, the containers are stored for at least 4 weeks before measurements in order to attain equilibrium between radium-226 and radon-222. Counting duration varies from 3 to 7 days according to sample activity. The energy window of interest lies between 40 keV (^{210}Pb at 46.7 keV) and 2700 keV (^{208}Tl at 2614.5 keV). The Th content is given by averaging all activities deduced from individual lines of ^{228}Ac, ^{212}Pb, ^{208}Tl and converted into mass concentration. In the U series, we distinguish 3 different sets of isotopes: firstly, the head of series, the corresponding U content which is noted U(^{238}U), is given by ^{234}Th, ^{234m}Pa and ^{235}U emissions; secondly, the immediate daughters of ^{226}Ra are given by ^{214}Pb and ^{214}Bi, the equivalent U content being noted U(^{226}Ra), assuming equilibrium between ^{222}Rn and ^{226}Ra; thirdly, the ^{210}Pb emission that leads to an equivalent U concentration noted U(^{210}Pb). The term "equivalent" illustrates the fact that the concentration in U is calculated from the corresponding isotopes, assuming secular equilibrium with their very first parents. These three values of U allow us to check and quantify the state of equilibrium between the different parts of the U decay series. K content is deduced from the single ^{40}K gamma line at 1460.8 keV. Calibration uncertainties are around 1% for K, U(^{238}U), U(^{226}Ra), Th, 5% for U(^{210}Pb).

The environmental dose rates measurements were carried out by NaI:Tl gammametry (see for instance Vieillevigne et al., 2007). We used a 2″×2″ NaI:Tl detector, interfaced with a Inspector 2000 Canberra 2 k channel portable analyzer (including HV supply). Spectra ranging from 0 to 10 MeV are recorded. The gamma component is deduced from the energy absorbed by the detector, integrated between 200 and 2650 keV (Guérin and Mercier, 2011). In addition, the gamma component is also deduced from the counts in the K (1461 keV), U (1765 keV) and Th (2615 keV) specific spectral windows. For the latter method, the spectral mode, the investigation thickness and the origin of the gamma rays (high energy gammas from the direct sources) are different from the former which is sensitive mainly to the Compton secondary gammas, as archaeological samples are. A significant deviation between both values can indicate non-homogeneity of the gamma radiation field. Moreover, high energy counts (more than 3 MeV) are generated by cosmic radiation (muon interactions with NaI) and the cosmic dose-rate is then also measured.

In order to check the homogeneity of the beta radiation field within a fragment of limestone, beta radiography analysis was performed using a high-speed image plate scanner CR 35 Bio (Dürr, Germany) which reads out the latent image of the imaging plate and converts it into a digital signal. This signal is turned into a greyscale image representing the spatial distribution of the signal produced on the imaging plate by the emitted radiation from the sample.

5. Results

5.1. Determination of equivalent doses

Fig. 2 displays the sets of TL curves obtained with sample BDX 14338b and BDX 14341b, after preheating and background subtraction. Natural and regenerated TL signals of BDX 14341b match perfectly indicating that annealing parameters were well adapted to that sample. On the other hand, with BDX 14338b we observe that the high temperature peak of Natural TL deviates from regenerated signals meaning that this sample was heated at a lower temperature in the past than the ceiling one. This is also confirmed by the plateau tests (Fig. 3). All of them except BDX 14338b are satisfying over the whole temperature range, including the external part of BDX 14338 that was directly exposed to the ancient fires. All TL signals were integrated within the common plateau region, ca. 290°C–340 °C.

Table 3 reports the results of TL measurements. First of all, we remark that the MANARS protocol provides very precise data, which is a result of the direct comparison between natural signals and regenerated ones and also of the reproducibility and brightness of emissions. Recycling ratios are very close to one and we do not observe any noticeable predose effects (Fig. 4). The choice of parameters was valid, particularly the combination of the heating rate (4 °C/s) with the maximal temperature attained during TL measurements (420 °C) that contributes to reproducing a similar resetting of the material at each step of the procedure. Except for the 'bedrock' facing sample from the *Galerie des Mégacéros*, which is the less heated material, the recovery tests that we carried out according to an added dose technique, are also very acceptable. So, we consider that the protocol employed does not induce significant sensitivity changes between the first glow and the following ones and we estimate that it is a convenient tool for dating.

Examples of growth curves are displayed in Fig. 5. The growth of the 300 °C TL peak is supralinear in accordance with literature data. Experimental points are regrouped closely around the growth function and the statistical standard deviations on EDs are generally below 2%. Differences between EDs from the two faces of the samples appear to be highly significant. We note that the external part of both samples (4–5 mm thick, Table 1) was more irradiated than the one which was in contact with the bedrock. Two different assumptions contribute to the explanation of that observation: i) the sediment that fills the archaeological layers is clayey and probably more radioactive than the limestone itself; ii) the presence of free radon in the atmosphere, that is a public health concern in such caves, can also be the source of supplementary irradiation. Both hypotheses will be discussed in detail hereafter, however, at the actual point of analysis, we can state that the most confident data will be given by the bedrock part of the samples since the external parts of the heated limestone fragments are likely to have been submitted to supplementary beta and or alpha irradiations that are difficult to quantify. The measured k-factors are close to 0.1 and both modes of measurements agree (mode 1, by an additive alpha irradiation to the natural one; mode 2, by regenerating TL with an alpha irradiation after thermal resetting of aliquots).

5.2. Radioactivity and annual dose assessment

Table 4 reports K, U and Th data of samples, as well as their water saturation contents. The very low content of K and Th is related to the low level of detritic phases of the Urgonian limestone. We observe the high activity of ^{210}Pb compared to ^{238}U and ^{226}Ra. Table 5 reports in situ measurements of environmental dose-rates. The spectra were also exploited to determine the apparent contents of U, Th and K in the vicinity of the gamma measurements. At the sample locations, the field gamma spectrum is dominated by that of U and more precisely by ^{214}Bi and ^{214}Pb emissions (U window around 1765 keV ^{214}Bi) which are short lifetime daughters of radon-222. The gamma environment at the entrance scree is rather heterogeneous as we can deduce from Table 5. On the contrary, at the *Galerie des Mégacéros*, the radiation field, seems more homogeneous in terms of dose rates due to the balance of radioelements between the wall (limestone, rich in U compared to K and Th) and the soil (rich in clay, then expectedly richer in K, and Th than

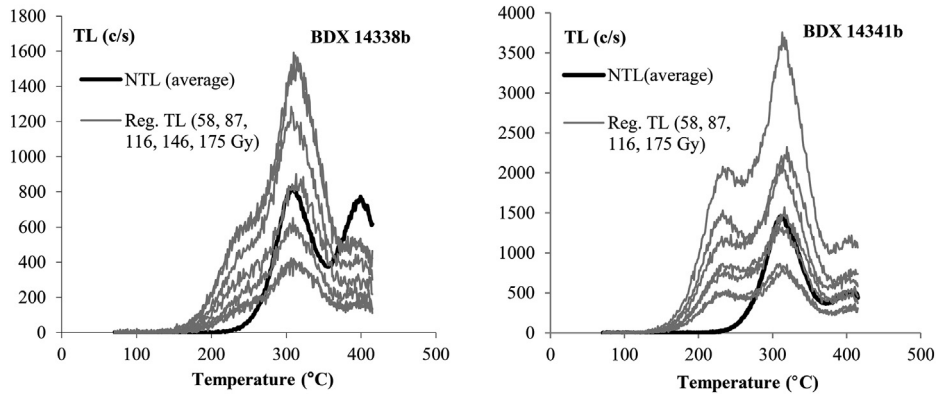

Fig. 2. TL curves after background subtraction and normalization of fine grained heated calcite from the walls of Chauvet Pont-d'Arc Cave. The natural signal corresponds to the mean TL curve. All experiments are performed in CO_2 with a heating-rate of 4 °C/s. The end point is 420 °C. Compared to literature, the TL peaks generally found at around 280 °C and 360 °C, appear at 300 °C and 390 °C respectively in our experiments.

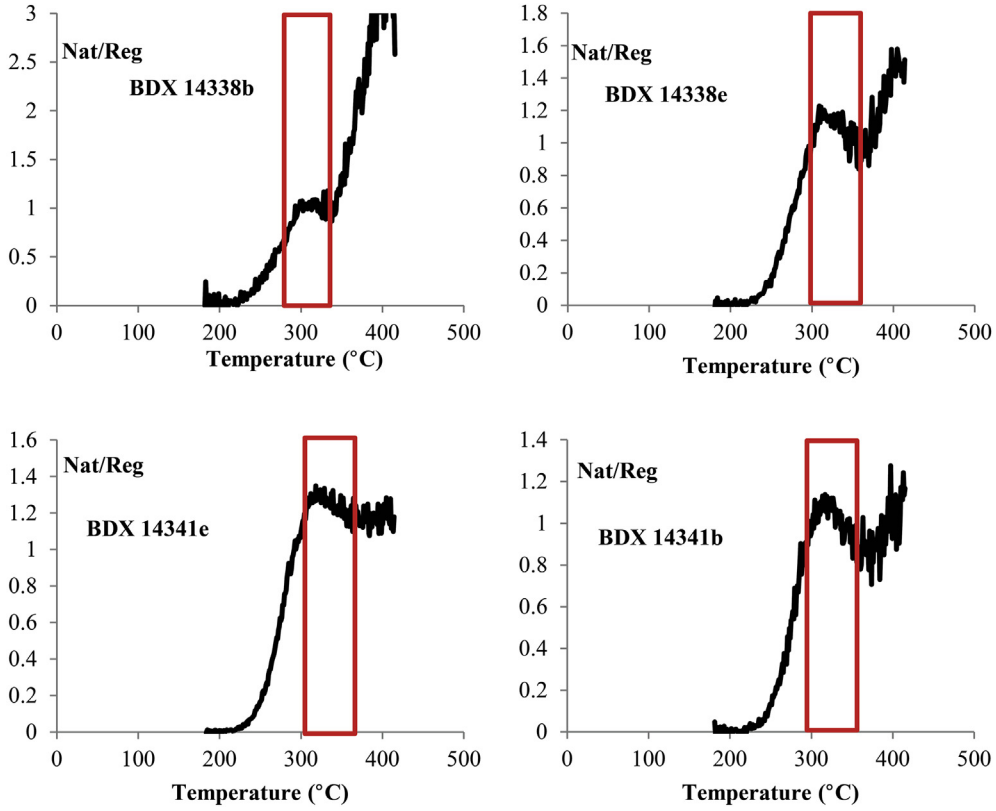

Fig. 3. Plateau tests: ratio Nat TL/Reg TL as a function of temperature and selected region of integration. All samples exhibit a plateau region around 290–340 °C that was used as a region of interest for age measurements. The important growth of the ratio Nat/Reg of subsample BDX 14338b beyond 340 °C reflects the fact that this part of the sample (in contact with the wall) was less heated in the past than the other subsample BDX 14338e, exposed to the flames of the paleolithic fires and which exhibits a better plateau.

limestone). All field data show an important amount of U (post-radon) by comparing with laboratory measurements of the limestone fragments (ca. 3–4 ppm for U(^{226}Ra), but larger activity of ^{210}Pb). We can thus deduce that a part of the gamma dose rate comes from radon and daughters. This is also consistent with the supplementary irradiation of the external parts of the dated samples that exhibit higher EDs than their 'bedrock' face, and that have integrated alpha and beta doses coming from the air.

According to the results of laboratory analysis, ^{210}Pb is in large excess in samples of limestone and this is particularly visible for the reference limestone fragment BDX 14342, the external faces of which were not removed during its physical preparation for gamma spectrometry (ratio ^{210}Pb/^{226}Ra of ca. 15 in this sample against 2.5–2.8 for the others). We recall that the half period of ^{210}Pb being 22y, the observed activity is the average value of this nuclide during the past 30y ($T_{1/2}$/ln(2)). It is produced by ^{222}Rn through a series of short life daughters.

A beta autoradiography was carried out to determine where excess ^{210}Pb is localized in limestones. The reference limestone fragment BDX 14342 was used as a possible model for the smaller chips being dated: a small cube (~15 mm long edges) was cut and was set on the imaging plate. The result is shown in Fig. 6. The

Table 3
Results of TL study (errors are statistical standard deviations only). The statistical errors are very low as a consequence of the direct comparative process of natural signals with the regenerated ones. The differences in ED between the two faces of each sample are very significant, the part facing the bedrock being less irradiated than the ones facing the soil. Recycling ratios are close to unity. The dose recovery tests (by an added dose technique) give also satisfactory results, except for subsample BDX 14348b, that deviates from unity. Actually, no significant predose effect was observed within the samples, meaning that the thermal zeroing process is adapted to the thermal history of these samples.

Sample	ED (Gy)	Recycling ratio	Recovery ratio (added dose)	Predose dependence	Alpha efficiency (k)	
					Mode 1	Mode 2
Wall of *Galerie des Mégacéros*						
BDX 14338b Facing wall	105.7 ± 0.7	0.991 ± 0.008	1.18 ± 0.02	No marked trend (less than ± 5%)	0.095 ± 0.005	0.100 ± 0.005
BDX 14338e Facing gallery and soil	120.2 ± 1.0	1.006 ± 0.008	1.03 ± 0.01		0.095 ± 0.005	0.084 ± 0.004
Ceiling of *Secteur de l'Entrée*						
BDX 14341e Facing soil	163.4 ± 1.0	0.98 ± 0.02	1.04 ± 0.01	Slight increase with dose	0.073 ± 0.004	0.083 ± 0.004
BDX 14341b Facing upper bedrock	85.7 ± 2.0	0.96 ± 0.02	0.96 ± 0.02		nd	0.100 ± 0.003

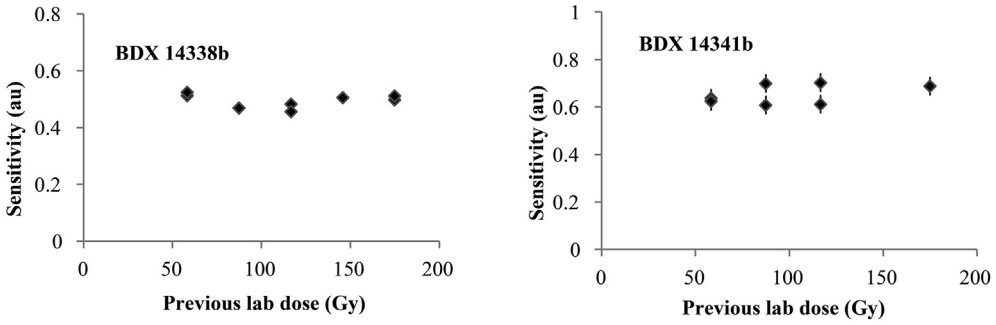

Fig. 4. Predose effects: plot of sensitivity vs regenerated dose. Within the statistical uncertainties, no significant sensitivity dependence with the previous irradiation can be observed.

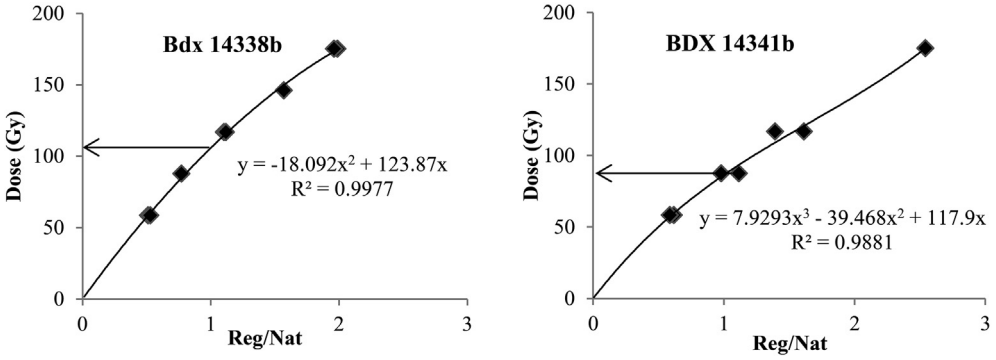

Fig. 5. Normalized growth curves and determination of ED following an unusual representation: normalized TL on X-axis, dose on the Y-axis (X = 1 represents the natural signal). The growth of TL with dose is supralinear and the segment studied is better fitted by polynomials than by a saturating exponential function.

Table 4
High resolution gamma spectrometry results and saturation water content (errors are one standard deviation). Concentrations in K and Th are very low, as a consequence of a very low level of detrital minerals within the Urgonian limestone. By constrast, U content is high and is the main source of internal irradiation within those samples. U and Ra are in equilibrium, but ^{210}Pb exhibits a very high activity compared to ^{238}U and ^{226}Ra.

Sample	K (%)	U(^{238}U) (ppm)	U(^{226}Ra) (ppm)	U(^{210}Pb) (ppm)	Th (ppm)	H_2O_{sat} (%)
BDX 14338 (*Galerie des Mégacéros*)	0.01 ± 0.01	3.98 ± 0.20	3.87 ± 0.06	9.59 ± 0.92	0.15 ± 0.10	3.1
BDX 14341 *(Secteur de l'Entrée*)	0.01 ± 0.01	2.63 ± 0.11	2.66 ± 0.03	7.50 ± 0.40	<0.10	5.7
BDX 14342 (unheated limestone)	<0.02	2.83 ± 0.18	2.54 ± 0.05	37.3 ± 1.7	0.19 ± 0.09	n.d.

darker dyes correspond to the most irradiated areas of the imaging plate. We note that the two external sides are the main sources of beta particles and the inside is rather homogeneous and less radioactive. Consequently, we assume that ^{210}Pb in excess is adsorbed mainly at the external surface of that sample. But, for the dated samples, despite the removal of their outer parts, ^{210}Pb in excess as gamma spectrometry measures it, implies also its real presence in the interior of the heated fragments.

Table 5
In situ measurements of environmental dose-rates. The main contribution is given by daughters of ^{226}Ra and ^{222}Rn in the U-series. The variation of the gamma dose-rate according to the precise location of the gamma probe is important, particularly at the paleoentrance area. The cosmic contribution is, as expected, very low, but significantly higher at the entrance than at the Megaceros Gallery.

Localization of measurement	$K_{eq.}$ (%)	$U_{eq.}$ (ppm)	$Th_{eq.}$ (ppm)	I_{cosmic} (Gy/ka)	I_{gamma} (Gy/ka)	I_{env} (Gy/ka)
Paleoentrance scree/Eboulis d'entrée						
Gamma probe close to the ceiling sample BDX 14341	0.1 ± 0.1	15.4 ± 1.4	<0.4	0.013 ± 0.004	1.26 ± 0.03	1.27 ± 0.03
Gamma probe on flowstone below sample location	0.35 ± 0.06	7.0 ± 0.5	1.38 ± 0.25	0.018 ± 0.003	0.72 ± 0.02	0.74 ± 0.02
Gamma probe on soil between limestone blocks	0.12 ± 0.07	8.0 ± 0.7	0.8 ± 0.3	0.012 ± 0.003	0.68 ± 0.02	0.69 ± 0.02
Megaloceros Gallery – Galerie des Mégacéros						
Gamma probe on wall close to sample BDX 14338	0.1 ± 0.1	12.2 ± 1.1	<0.4	0.005 ± 0.002	1.04 ± 0.03	1.05 ± 0.03
Gamma probe on soil. near a limestone block and cave bear skeleton	0.61 ± 0.08	10.5 ± 0.8	2.9 ± 0.4	0.007 ± 0.002	1.18 ± 0.03	1.19 ± 0.03

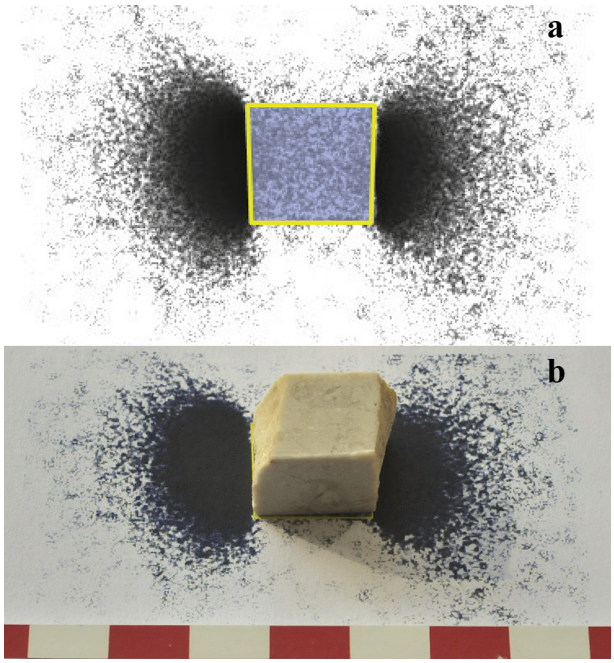

Fig. 6. Beta Autoradiography image (Fig. 6a) and its interpretation: in the lower figure (Fig. 6b), the sample has been set on a scaled print out of the radiography image in its original position. The limestone cube presents two natural faces (the lateral left and right sub vertical ones) and four cut faces, the inferior one being in contact with the imaging plate.

6. Discussion and conclusions

6.1. About the excess of radon and its consequence on dose rate

The presence of free radon in the karst addresses new questions about its possible variations with time and their consequences on paleodosimetry. First of all, although we do not know precisely the relative importance of the free radon and daughters in the gamma dose rate, it is expected to be significant and therefore it is important to evaluate the seasonal variability of Rn concentration in the air knowing that our field measurements were made during the early spring period in 2011 and 2012 (end March, beginning of April). To evaluate the appropriateness of our measurements, we examined previous reports on continuous survey of Rn and CO_2 that were undertaken at the Chauvet-Pont d'Arc Cave (Mangin and d'Hulst, 2005; Marie et al., 2007; Bourges et al., 2010). The concentration of radon fluctuates with the external temperature: in summer, the radon activity is higher than in winter (winter 6700 Bq/m^3 – summer 8900 Bq/m^3 in 2009 in the *salle Hilaire*, one of the chambers in connection with the *Galerie des Mégacéros*). A weak dependence with the atmospheric pressure was also observed (the higher the pressure, the less the radon concentration). The early spring, according to the reported data, corresponds to median values of radon. It is therefore meaningful to use them without any seasonal corrections to get the average value of the gamma dose rate. Long term variations cannot be evaluated consistently, but we can imagine that the positively correlated temperature dependence of the radon concentration makes a lower concentration during the ice age possible. It is also closely dependent on the natural system of air renewal in the cave and that aspect remains unknown, except for the fact that the cave was definitely closed 21.5 ± 1.0 ky ago (Sadier et al., 2012), the time of the final episode of collapses of the upper cliff.

To calculate the internal (alpha and beta) dose rate of the heated fragments of limestone, we used the concentration data given by gamma-spectrometric measurements on the one hand and in situ environmental dose rate measurements on the other hand. The presence of ^{210}Pb in excess inside the dated limestone chips makes two different scenarios possible that lead to major differences in dose rates, either ^{222}Rn and daughters or ^{210}Pb and daughters are in excess within the rock. Firstly, we examine the possibility of an excess of ^{222}Rn.

The origin of radon in the air of the cave is the result of both absence of natural ventilation and radon emanation from the bedrock, from the karstic clay materials, and also perhaps from silicated basement through the Mesozoic faulted beds. The dependence of radon concentration on the external temperature tends however to demonstrate that the main part of the radon is of local origin, and that is the assumption upon which we based our further discussion. In general, radon activity is counterbalanced by its radioactive decay. To characterize the potential radon escape from a material, a parameter, the emanation factor, has been designed by specialists (Abumurad and Al-Tamimi, 2001; Bossew, 2003; Sakoda et al., 2011). The emanation factor is the proportion of mobile radon, generally produced at the surface of a grain containing ^{226}Ra, to the concentration of radon in a given dried medium. This factor is below 2% in limestone (grained to 125–250 μm), extremely variable but around 20% in soil (with grain size < 40 μm), according to Sakoda et al. review paper (2011). If we only consider the limestone bedrock, under the condition that the published values for limestone are also valid for the Chauvet Urgonian limestone bedrock, 2% of the ^{222}Rn produced is able to escape from any volume of rock. In our case, 4 ppm of U(^{226}Ra) leads to ca. 50Bq/kg of rock, meaning that 1Bq/kg is able to migrate in the pores which represent around 10% of the limestone volume (deduced from saturation wt% of water in dated samples: 3.1 and 5.7%). If 1Bq/kg of free radon from limestone is capable of being mixed with the corresponding air volume of pores (10% of 400 cm^3 roughly is 40 cm^3) the maximal radon activity in rock air should be around 25kBq/m^3, nearly 4 times more than the air activity measured in the Chauvet-Pont d'Arc Cave (around 7kBq/m^3). The expected behavior of mobile radon produced in the bedrock is thus escape to the galleries, by molecular diffusion in air towards the less

concentrated areas, rather than penetrating the walls from the surface. A similar diffusion mechanism can also take place in pore water, if we suppose that the pores are filled with water, with a degassing process at the surface of the rock.

The chemical properties of lead ions being very different to those of radon atoms (chemically inert), we must mention other mechanisms for an enrichment in ^{210}Pb. Migration of radon towards the exterior of the bedrock should have enriched the pores with its longer life daughter ^{210}Pb during the last 3 decades (mean age of continuously produced ^{210}Pb atoms) by ionic adsorption on grain surface or co-precipitation with newly formed calcium carbonate phases, that are very likely mechanisms. At the surface, the evaporation process of water transporting dissolved radon and ^{210}Pb ions can occur and may also provoke a high activity surface deposit of ^{210}Pb. In reverse, ions of ^{210}Pb or earlier daughters of ^{222}Rn that are produced in air can also be fixed at the surface of the bedrock. Diffusion processes inside the bedrock according to ionic diffusion in aqueous medium can also occur provided that the concentration in lead ions of the rock water in pores is lower than at the surface. Both ways of apparent migration of ^{210}Pb, to the inside or to the exterior, can enrich ^{210}Pb at the surface and inside the rock, near the surface.

We can then interpret an excess of ^{210}Pb inside both dated samples as the result of a mid-term transport of ^{210}Pb inside the rock. A more detailed characterization of a profile of ^{210}Pb inside the bedrock should be useful and necessary in the future to overcome the remaining uncertainties and to improve the understanding of the exchange of radon and daughters between walls and air. Moreover, we have considered that the excess presence of radon and daughters has occurred since the closure of the Chauvet-Pont d'Arc Cave, due to the lack of air renewal. So, to calculate the mean dose rate, we took account of a two-phase irradiation model: before closure, radon and daughters are supposed as being in equilibrium with ^{226}Ra, and after closure, the actual state of disequilibrium and dose-rate is attained. The part played by radon and daughters in the gamma dose rate was not evaluated. It seems that the major part of the emitting environment should be composed by the bedrock and the filling sediment, but the high activity of air, 7kBq/m^3, indicates that the radioactivity of the air volume in the galleries cannot be totally neglected in the dosimetric assessment. To take account of possible errors in gamma dose rate estimation and its variations over time, we finally attributed an arbitrary systematic uncertainty of 10% to the measured value. Tables 6 and 7 respectively report the annual dose rate factors used and values of the different components of the annual dose according to the situation of the Paleolithic entrance.

6.2. Dating results and conclusions

The final TL ages are dependent on the date of closure of the cave if we assume that the excess of ^{210}Pb and ^{222}Rn are the result of an absence of ventilation, even at the *Galerie des Mégaceros*. The TL age, t, is given by the following relation (R1):

$$t = \frac{\{ED - (I_2 - I_1)t_{closure}\}}{I_1} \quad (R1)$$

with ED the measured equivalent dose, $t_{closure}$ the age of closure of the cave; I_1 and I_2 are dose rates before and after closure respectively. The obvious condition that the closure age must be lower than the fires is to be fulfilled. Of course, radiocarbon dates on charcoals also give upper limits to the human occupation of the cave, and cosmonuclides data give the final answer for the last collapse of the cliff and thus for the closure. We found the following TL ages and total standard deviations (in brackets statistical std. dev.):

- BDX 14338b, *Galerie des Mégacéros*, 36.9 ± 2.3 ka (stat: 0.9 ka),
- BDX 14341b, *Eboulis d'entrée*, 34.3 ± 2.9 ka (stat: 1.0 ka)

Even if the statistical errors on age determination are apparently low, due to the precision of the ED TL measurement process, the estimated systematic errors due to calibration errors and also possible variations of gamma dose-rates with the time increase the total of the uncertainties. Finally, dating by TL heated fragments of rock from the walls of the Chauvet-Pont d'Arc Cave was a challenging operation due to the rarity of the materials and to the fact that we could not sample this site extensively. Moreover, the complexity of the irradiation field which was firstly evidenced by the excess of ^{210}Pb was attributed to radon emanation and its accumulation in the cave. We must keep in mind that the calculated dose-rate and final age are dependent on the model used, and, here, more peculiarly, to the fact that we supposed that ^{210}Pb in excess and daughters were distributed uniformly inside the two samples studied and not only at their outer surfaces.

However, these TL ages are consistent with the set of calibrated radiocarbon densities obtained both in the *Galerie des Mégacéros* (Valladas et al., 2001b, 2005) and in the excavation pit at the Paleolithic Entrance (Delannoy et al., 2010). They indicate that the two dated fires that burnt the walls at the Chauvet-Pont d'Arc Cave

Table 6
Specific annual dose rates from Guérin et al. (2011) expressed in Gy/ka per 1 ppm U and Th, and per 1% K. For U series, 3 sets of isotopes were taken into account according to the model discussed in this paper. Within each set, all nuclides are supposed to be in secular equilibrium.

Radioelement and content unit	Alpha	Beta	Gamma	Series of radionuclides involved
U(^{238}U) ppm	0.571	0.056	0.0017	^{238}U → ^{234}U and ^{235}U → ^{231}Th
U(^{226}Ra) ppm	1.893	0.0632	0.1096	^{230}Th → ^{214}Po and ^{231}Pa → ^{207}Pb
U(^{210}Pb) ppm	0.331	0.0264	0.0003	^{210}Pb → ^{206}Pb
Th ppm	0.738	0.0277	0.0479	^{232}Th → ^{208}Pb
K %		0.798	0.249	^{40}K → ^{40}Ar,^{40}Ca

Table 7
Summary of annual dose components (errors are total standard deviation, quadratic sum of statistical and systematic uncertainties) of the samples dated. It is assumed that the closure of the cave leads to a supplementary irradiation linked with the retention of radon and daughters inside the karstic network.

Sample	kI_α (Gy/ka)	I_β (Gy/ka)	I_{env} (Gy/ka)	I_{total} (Gy/ka)
BDX 14338b before closure	1.07 ± 0.07	0.56 ± 0.02	1.05 ± 0.10	2.67 ± 0.14
BDX 14338b after closure	1.25 ± 0.08	0.71 ± 0.04	1.05 ± 0.10	3.00 ± 0.15
BDX 14341b before closure	0.70 ± 0.03	0.37 ± 0.02	1.27 ± 0.13	2.34 ± 0.14
BDX 14341b after closure	0.85 ± 0.04	0.49 ± 0.05	1.27 ± 0.13	2.62 ± 0.15

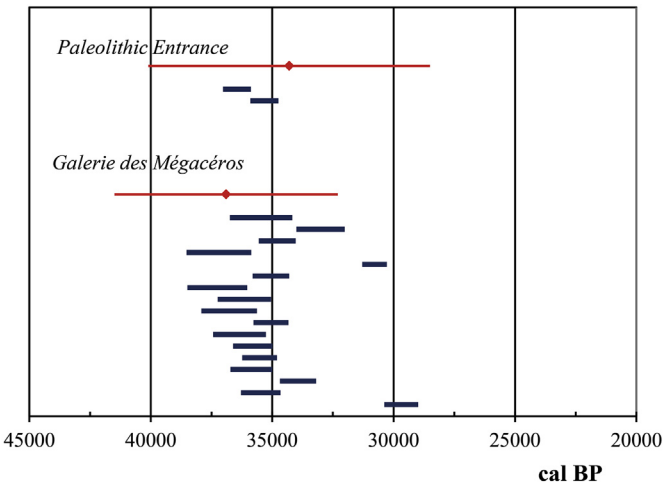

Fig. 7. Calibrated radiocarbon (using IntCal13, Reimer et al., 2013) results from charcoals collected in the *Galerie des Mégacéros* and in an excavation pit near the *Eboulis d'entrée* (95% confidence interval), compared to TL dates of heated walls (error bars for TL represent ± 2 total standard deviations).

can be as old as the first prehistoric occupation, defined by a set of radiocarbon dates obtained from drawings and ground charcoal pieces (Fig. 7, supplementary table S3). Finally, the demonstration of an anthropic rubefaction of walls by heating is now complete, since we have been able to determine an evaluation of a heating age consistent with one of the human occupations of the Chauvet-Pont d'Arc Cave, and actually the earlier period, assigned to Aurignacian people. Beyond these first results, dating heated calcite from the thermally treated parts of the Chauvet-Pont d'Arc bedrock, in close stratigraphic relation with drawings and engravings, opens up new possibilities of dating the rock art at Chauvet-Pont d'Arc, and it could be extended at any ornamented cave site that also displays a thermal process of its walls.

Acknowledgments

The authors are very grateful to the colleagues who indirectly made this study possible: Stéphan Dubernet (Engineer at the Univ Bordeaux Montaigne) responsible for the important task concerning the authorization to use radioactive sources at the IRAMAT-CRP2A, Pierre Selva (Engineer at the CNRS) for his assistance and maintenance of the TL machines. We also acknowledge Loïc Martin, PhD student at the IRAMAT-CRP2A for his help in beta imaging development, and Bertrand Kervazo, geologist, now retired, for all his important contribution to the study of the Chauvet–Pont d'Arc cave.

This work was supported financially by the University Bordeaux Montaigne (Aurélie Brodard's PhD grant, the study of Chauvet samples was a part of her work), by the French Ministry of Culture and Communication (*Opération* Chauvet) and by the labex LaScArBx (label of excellence Archaeological Sciences Bordeaux) according to the general program supported by the ANR (Agence Nationale de la Recherche) - n°ANR-10-LABX-52. The equipments used were co-financed by multiple fundings including the Conseil Régional d'Aquitaine, the CNRS, the labex LaScArBx, the French Ministry of Research and Higher Education.

Appendix A. Supplementary data

Supplementary data related to this article can be found at http://dx.doi.org/10.1016/j.quageo.2015.04.007.

References

Abumurad, K.M., Al-Tamim, M., 2001. Emanation power of radon and its concentration in soil and rocks. Radiat. Meas. 34, 423–426.
Aitken, M.J., 1985. Thermoluminescence Dating. Academic Press, London, p. 359.
Bassinet, C., Mercier, N., Miallier, D., Pilleyre, T., Sanzelle, S., Valladas, H., 2006. Thermoluminescence of heated quartz grains: Intercomparisons between SAR and multiple-aliquot additive dose techniques. Radiat. Meas. 41, 803–808.
Blain, S., Guibert, P., Bouvier, A., Vieillevigne, E., Bechtel, F., Sapin, C., Baylé, M., 2007. TL-dating applied to building archaeology: the case of the medieval church Notre-Dame-Sous-Terre (Mont-Saint-Michel, France). Radiat. Meas. 42, 1483–1491.
Bocherens, H.G., Drucker, D.G., Billiou, B., Geneste, J.M., van der Plicht, J., 2005. Bears and humans in Chauvet Cave (Vallon-Pont-d'Arc, Ardèche, France): insights from stable isotopes and radiocarbon dating of bone collagen. J. Hum. Evol. 50, 370–376. http://dx.doi.org/10.1016/j.jhevol.2005.12.002.
Bon, C., Berthonaud, V., Fosse, P., Gély, B., Maksud, F., Vitalis, R., Philippe, M., van der Plicht, J., Elalouf, J.M., 2011. Low regional diversity of late cave bears mitochondrial DNA at the time of Chauvet Aurignacian paintings. J. Archaeol. Sci. 38, 1886–1895.
Bossew, P., 2003. The radon emanation power of building materials, soil and rocks. Appl. Radiat. Isotopes 59, 389–392.
Bourges, F., Mangin, A., d'Hulst, D., 2010. Suivi environnemental et études sur la grotte Chauvet-Pont d'Arc, p. 16. Report 2009-2010 for the Conservation Régionale des Monuments Historiques Rhône-Alpes.
Brodard, A., Guibert, P., Ferrier, C., Debard, E., Kervazo, B., Geneste, J.M., 2014. Les rubéfactions des parois de la grotte Chauvet : une histoire de chauffe? In: Paillet, P. (Ed.), Les arts de la Préhistoire : micro-analyses, mises en contextes et conservation, Proceedings of the seminar « Micro-analyses et datations de l'art préhistorique dans son contexte archéologique », MADAPCA – Paris, 16-18 novembre 2011, PALEO, special issue, 2014, pp. 233–235.
Carmichael, L.A., Sanderson, D.C.W., Ni Riain, S., 1994. Thermoluminescence measurements of calcite shells. Radiat. Meas. 23 (2/3), 455–463.
Cuzange, M.T., Delqué-Količ, E., Tomasz Goslar, T., Meiert Grootes, P., Higham, T., Kaltnecker, E., Nadeau, M.J., Oberlin, C., Paterne, M., van der Plicht, J., Bronk Ramsey, C., Valladas, H., Clottes, J., Geneste, J.M., 2007. Radiocarbon intercomparison program for Chauvet Cave. Radiocarbon 49 (2), 339–347.
Delannoy, J.J., Sadier, B., Jaillet, S., Ployon, E., Geneste, J.M., 2010. Reconstitution de l'entrée préhistorique de la grotte Chauvet-Pont d'Arc (Ardèche, France) : les apports de l'analyse géomorphologique et de la modélisation 3D. Karstologia 56, 21–38.
Duttine, M., Guibert, P., Perraut, A., Lahaye, C., Bechtel, F., Villeneuve, G., 2005. Effects of thermal treatments on TL and EPR of flints and their importance in TL-dating : application to french Mousterian sites of Les Forêts (Dordogne) and Jiboui (Drôme). Radiat. Meas. 39 (4), 375–385.
Engin, B., Güven, O., 1997. Thermoluminescence dating of Denizli Travertines from the Southwestern part of Turkey. Appl. Radiat. Isotopes 48 (9), 1257–1264.
Engin, B., Güven, O., 2000. The effect of heat treatment on the thermoluminescence of naturally-occuring calcites and their use as a gamma-ray dosimeter. Radiat. Meas. 32, 253–272.
Ferrier, C., Debard, E., Kervazo, B., Brodard, A., Guibert, P., Baffier, D., Feruglio, V., Gély, B., Geneste, J.M., Maksud, F., 2014. Les parois chauffées de la grotte Chauvet-Pont d'Arc (Ardèche, France) : caractérisation et chronologie. PALEO 25, 59–78.
Franklin, A.D., Hornyak, W.F., Pagonis, V., Kristianpoller, N., 1990. Thermoluminescence study of annealing a geological calcite. Nucl. Tracks Radiat. Meas. 17 (4), 517–523.
Ganteaume, M., Baumer, A., Lapraz, D., Iacconi, P., Bokilo, J.E., Bernat, M., Zahra, C., 1990. La transformation aragonite-calcite dans les coraux fossiles, relation avec la thermoluminescence. Thermochim. Acta 170, 121–137.
Genty, D., Ghaleb, B., Plagnes, V., Causse, C.H., Blamart, D., Massault, M., Geneste, J.M., Clottes, J., 2004. Datations U/Th (TIMS) et 14C (AMS) des stalagmites de la grotte Chauvet (Ardèche, France) : intérêt pour la chronologie des événements naturels et anthropiques de la grotte. Palevol 3, 629–642.
Guérin, G., Mercier, N., 2011. Determining gamma dose rates by field gamma spectroscopy in sedimentary media: results of Monte Carlo simulations. Radiat. Meas. 46 (2), 190–195.
Guérin, G., Mercier, N., Adamiec, G., 2011. Dose-rate conversion factors: update. Anc. TL 29, 5–8.
Guibert, P., 2002. progrès récents et perspectives. Habilitation à diriger des recherches, 10 juillet 2002. Datation par thermoluminescence des archéomatériaux : recherches méthodologiques et appliquées en archéologie médiévale et en archéologie préhistorique, 3. Université de Bordeaux, p. 180.
Guibert, P., Bailiff, I.K., Blain, S., Gueli, A.M., Martini, M., Sibilia, E., Stella, G., Troja, S.O., 2009a. Luminescence dating of architectural ceramics from an early medieval abbey: the St-Philbert intercomparison (Loire-Atlantique, France). Radiat. Meas. 44 (5–6), 488–493.
Guibert, P., Lahaye, C., Bechtel, F., 2009b. The importance of U-series disequilibrium of sediments in luminescence dating: a case study at the Roc de Marsal cave (Dordogne, France). Radiat. Meas. 44, 223–231.
Joannes-Boyau, R., Scheffers, A., Chapoulie, R., Lahaye, C., Parr, J., Orange, M., Moffat, I., Guibert, P., 2014. Thermal behavior of organic radicals and paramagnetic centres in chert: a case study of Bergeracois brown chert, Dordogne, France. Quat. Geochronol. 23, 26–34.

Macedo, M.S., Valerio, M.E.G., de Lima, J.F., 1999. Thermoluminescence mechanism of Mn^{2+}, Mg^{2+} and Sr^{2+} doped calcite. J. Phys. Chem. Solids 60, 1973–1981.
Mangin, A., d'Hulst, D., Bourges, F., 2005. Etude de l'environnement souterrain de la Grotte Chauvet – Suivi annuel des concentrations en radon, p. 12. Report for the Conservation Régionale des Monuments Historiques Rhône-Alpes.
Marie, L., Améon, R., Diez, O., Dupuis, M., 2007. Le radon dans les grottes ornées – campagne de mesures estivale et synthèse de l'étude, p. 27. Report IRSN/DEI/SARG/2007-005.
Nakajima, T., 1971. Influence of OH anion on the thermoluminescence yields of some phosphors. In: Proceedings of the 3rd International Conference on Luminescence Dosimetry, AEC Risoe, p. 90.
Ninagawa, K., Kitahara, T., Toyoda, S., Hayashi, K., Nishido, H., Kinjo, M., Kawana, T., 2001. Thermoluminescence dating of the Ryukyu Limestone. Quat. Sci. Rev. 20, 829–833.
Ninagawa, K., Matsukuma, Y., Fukuda, T., Sato, A., Hoshinoo, N., Nakagawa, M., Yamamoto, I., Wada, T., Yamashita, Y., Sekimoto, K., Komura, K., 1994. Thermoluminescence dating of calcite shells, Crassostrea gigas (Thunberg) in the Ostreidae family. Quat. Geochronol. 13, 589–593.
Pagonis, V., 1998. The effect of annealing atmosphere on the thermoluminescence of synthetic calcite. Radiat. Meas. 29 (1), 45–52.
Pagonis, V., Michael, C., 1994. Annealing effects on the thermoluminescence of synthetic calcite powder. Radiat. Meas. 23 (1), 131–142.
Pettitt, P., 2008. Art and the Middle-to-Upper Paleolithic transition in Europe: comments on the archaeological arguments for an early Upper Paleolithic antiquity of the Grotte Chauvet art. J. Hum. Evol. 55, 908–917.
Polikreti, K., Michael, C.T., Maniatis, Y., 2003. Thermoluminescence characteristics of marble and dating of freshly excavated marble objects. Radiat. Meas. 37, 87–94.
Ponnusamy, V., Ramasamy, V., Jose, M.T., Anandalakshmi, K., 2012. Effect of annealing on natural calcitic crystals, a thermostimulated (TSL) study. J. Luminescence 132, 1063–1075.
Quiles, A., Valladas, H., Geneste, J.M., Clottes, J., Baffier, D., Berthier, B., Brock, F., Bronk Ramsey, C., Delqué-Količ, E., Dumoulin, J.P., Hajdas, I., Hippe, K., Hodgins, G.W.L., Hogg, A., Jull, A.J.T., Kaltnecker, E., de Martino, M., Oberlin, C., Petchey, F., Steier, P., Synal, H.A., van der Plicht, J., Wild, E.M., Zazzo, A., 2014. Second intercomparison program for the Chauvet Pont-d'Arc Cave Ardèche France. Radiocarbon 56 (2), 833–850.
Reimer, P.J., Bard, E., Bayliss, A., Beck, J.W., Blackwell, P.G., Bronk Ramsey, C., Grootes, P.M., Guilderson, T.P., Haflidason, H., Hajdas, I., Hatté, C., Heaton, T.J., Hoffmann, D.L., Hogg, A.G., Hughen, K.A., Kaiser, K.F., Kromer, B., Manning, S.W., Niu, M., Reimer, R.W., Richards, D.A., Scott, E.M., Southon, J.R., Staff, R.A., Turney, C.S.M., van der Plicht, J., 2013. IntCal13 and Marine13 radiocarbon age calibration curves 0-50,000 Years cal BP. Radiocarbon 55 (4), 1869–1887.
Roque, C., Guibert, P., Vartanian, E., Bechtel, F., Schvoerer, M., 2001a. Thermoluminescence - dating of calcite: study of heated limestone fragments from Upper Paleolithic layers at Combe-Saunière, Dordogne, France. Quat. Sci. Rev. 20, 935–938.
Roque, C., Guibert, P., Vartanian, E., Bechtel, F., Oberlin, C., Evin, J., Mercier, N., Valladas, H., Texier, J.P., Rigaud, J.P., Delpech, F., Cleyet-Merle, J.J., Turq, A., 2001b. Une expérience de croisement de datations TL/14C pour la séquence solutréenne de Laugerie-Haute, Dordogne. In: Barrandon, Dir. J.-N., Guibert, P., Michel, et V. (Eds.), Datation, XXIe Rencontres Internationales d'Archéologie et d'Histoire d'Antibes. Editions APDCA, Antibes, pp. 217–232.
Roque, C., Guibert, P., Duttine, M., Vartanian, E., Chapoulie, R., Bechtel, F., 2004. Dependence of luminescence characteristics of irradiated quartz with thermal treatment and consequences for TL-dating: application to dating of Solutrean heated quartz pebbles from Laugerie Haute (Dordogne, France). Geochronometria 23, 1–8.
Sadier, B., Delannoy, J.J., Benedetti, L., Bourlès, D.L., Jaillet, S., Geneste, J.M., Lebatard, A.E., Arnold, M., 2012. Further constraints on the Chauvet Cave artwork elaboration. PNAS 109 (21), 8002–8006.
Sakoda, A., Ishimori, Y., Yamaoka, K., 2011. A comprehensive review of radon emanation measurements for mineral, rock, soil, mill tailing and fly ash. Appl. Radiat. Isotopes 69, 1422–1435.
Silletti, D.K., Brokus, S.A., Earlywine, E.B., Borycz, J.D., Peaslee, G.F., DeYoung, P.A., Peters, N.J., Robertson, J. David, Buscaglia, J.A., 2012. Radiation induced cathodoluminescent signatures in calcite. Radiat. Meas. 47, 195–200.
Townsend, P.D., Luff, B.J., Wood, R.A., 1994. Mn2+ transitions in the TL emission spectra of calcite. Radiat. Meas. 23 (2/3), 433–440.
Valladas, H., Clottes, J., Geneste, J.M., Garcia, M.A., Arnold, M., Cachier, H., Tisnérat-Laborde, N., 2001a. Evolution of prehistoric cave art. Nature 413, 479–479.
Valladas, H., Tisnérat-Laborde, N., Cachier, H., Arnold, M., Bernaldo de Quirós, F., Cabrear-Valdès, V., Clottes, J., Courtin, J., Fortea-Pérez, J.-J., Gonzàles-Sainz, C., Moure-Romanillo, A., 2001b. Radiocarbon AMS dates for paleolithic cave paintings. Radiocarbon 43 (2B), 977–986.
Valladas, H., Tisnérat-Laborde, N., Cacher, H., Kaltnecker, É., Arnold, M., Oberlin, C., Évin, J., 2005. Bilan des datations carbone 14 effectuées sur des charbons de bois de la grotte Chauvet. Bull. la Société Préhistorique Française 102 (1), 109–113.
Vieillevigne, E., Guibert, P., Bechtel, F., 2007. Luminescence chronology of the medieval citadel of Termez, Uzbekistan: TL dating of bricks masonries. J. Archaeol. Sci. 24, 1402–1416.